Brightest Cluster Galaxy Evolution Exploration: Comparing the Separation of Cluster X-ray Light and Visible Wavelength Galaxy Light with Spectral Data

A Senior Project
presented to
the Faculty of the Physics Department
California Polytechnic State University – San Luis Obispo

In Partial Fulfillment
of the Requirements for the Degree
Physics B.S.

By

Matthew Salinas

19 July 2019

Mon. Not. R. Astron. Soc. **000**, 000–000 (0000) Printed 19 July 2019 (MN LATEX style file v2.2)

Brightest Cluster Galaxy Evolution Exploration: Comparing the Separation of Cluster X-ray Light and Visible Wavelength Galaxy Light with Spectral Data

Matthew A. Salinas[1]⋆, Louise O.V. Edwards [1]†
[1]*Department of Physics, California Polytechnic State University, San Luis Obispo, CA*

19 July 2019

ABSTRACT
Brightest Cluster Galaxies (BCGs), the brightest galaxy in a cluster of hundreds to thousands of galaxies, are some of the biggest, brightest, and most massive galaxies in the universe. Characterizing a BCG can help discover more about galaxy evolution - the aging, changing, and possible merging (collisions) of galaxies. This project involves determining the separation of the peak of x-ray emission of the galaxy cluster, and the peak of visible emission of the BCG to characterize the system as being disturbed or undisturbed that can then lead to discoveries about its formation and evolution. We have found that 17.4% of the systems have large separations, and thus may have undergone a recent merging event. By comparing to previously published data, we can better define, more accurately classify, and further explain BCGs. More so, through analysis of the marriage of the results from spectra - like chemical composition, age, and velocities - and the differences in centroid distance, we can attain conclusions about each galaxy, or possibly determine any existing relationship among galaxies with disturbed states. This document highlights the steps undertaken to get images and data from databases, to create X-ray contours, and to overlay them on optical images. A discussion of locating and gathering the centroids of both the X-ray and optical images, steps to begin analysis, including learning how to use Jupyter notebook is also included. The analysis includes creating multiple histograms, and a comparison with previously published data.

Key words: galaxies: evolution; galaxies: interactions; galaxies:cD; galaxies: clusters.

1 INTRODUCTION

Brightest Cluster Galaxies (BCGs), the brightest galaxy in a cluster of hundreds to thousands of galaxies, are some of the biggest, brightest, and most massive galaxies in the universe. The galaxy's approximate center, also known as the centroid, can be found using visible images due to the emission of visible light from the stars within the BCG. On a similar note, the peak of X-ray wavelength light, which is emitted from the hot hydrogen gas dispersed throughout the cluster, can help determine the clusters' centroids. Characterizing and classifying the BCG's difference in centroid position can lead to discoveries about its formation and evolution through spectral data. Spectroscopy can tell us more about the chemical composition, age, and other characteristics about the BCGs. As part of this project, 7 new galaxies to the dataset were observed and reduced, listed in Table 1.

Characterizing a BCG can help discover more about galaxy evolution - the aging, changing, and possible merging (collisions) of galaxies. Learning about BCGs, some of the most massive structures in the universe, might provide insight about the adhesion of Dark Matter due to the presence of it in large amounts, to the structure of the gravitational potential well that is the galaxy cluster, about neighborhoods in the universe different than our own, and about the future of the BCG that is present near the centroid of the cluster. Analysis of the composition of BCGs in regards to the position between the two centroids can tell us more about mergers, like the one that the Milky Way and Andromeda galaxies will inevitably experience billions of years from now. By comparing our centroid positions to previously published data, such as Lakhchaura & Singh (2014) and Ebeling et al. (1996) and Ebeling et al. (2000), we can better define, more accurately classify, and further explain BCGs. The results from Lakhchaura and Singh include several galaxies, that are bothin this project and their Chandra study. The results from Ebeling include RASS X-ray centroids of 22 of our 23 clusters. Comparing my data and results with theirs will allow us to better define and classify BCGs. Edwards et al. (2016).

Using DS9, the peak of X-ray and visible emission - the centroids - were found. By recording these positions and finding their separation in different sources, the separation of the 23 BCGs was

⋆ E-mail:msalin03@calpoly.edu
† Advisor: Dr. Louise O.V. Edwards

determined and grouped based on their similarities in separation value. This included data that was reduced from observation from December 2016, Table 1. Using data received from reduced images of spectra, we can determine the age, redshift, and metallicity of these BCGs. We were then able to relate different properties of the BCG and cluster to others in order to search for a correlation, perhaps between separation and age of stars in the BCG.

The misalignment of the X-ray light peak (the centroid of the galaxy cluster) and the visible light peak (the centroid of the BCG) can indicate the results of a recent galaxy or cluster merger, indicating whether the cluster is in a disturbed or relaxed state. The marriage of the results from spectra from data reduction and the results from the separations of different BCGs can indicate a certain timeline the BCG underwent in order to be the way it currently is. If the BCG is located at the core of the cluster, it has likely been undisturbed for millennia; if it is offset, this indicates a recent disturbance, on the cosmological scale. Further analysis of this data and the differences in centroid distance, we can attain conclusions about each galaxy, or if there is any relationship among galaxies with disturbed states. Lauer et al. (2014) Lavoie et al. (2016)

2 DATA AND OBSERVATIONS

The command line, IRAF, and Python are used to analyze data gathered for this project. As a result, learning how to navigate and use commands, such as copying and moving data, via the course on Codecademy, was assigned. This campaign was the final run of 4 observing campaigns, measuring a total of 23 clusters. Below, we discuss the data reduction for the final 7 clusters.

2.1 Integral Field Spectroscopy from Sparsepak on WIYN

In this section, spectroscopy of 7 clusters observed using Sparsepak on WIYN in the beginning of December 2016 is discussed. Table 1 presents the galaxies from that observation. In Table 1, there are 6 columns. The first column addresses each of clusters' name. The second column records the date of observation using Sparsepak. The third and fourth columns provide the Right Ascension and Declination respectively, coordinates of the objects. The fifth column lists the number of images taken, while the sixth has the exposure time of the images.

Because there were two of us doing the analysis, we split the data we had in about half. The author did Home A160A, Home A0602, Home A0671, Home A0757, Offset1 A0602, Offset1 A160A, Offset1 A0757, Offset2 A0602, Offset2 A160A, and

Table 1. Galaxy Clusters Observed by Sparsepak by on the final data run. A table that presents the galaxies we reduced data for. I reduced the data of first 4 clusters, indicated with an asterisk.

Cluster	Date	RA	Dec	#	IT (s)
-A602	12-05-16	+07:53:26.685	+29:21:33.590	3	900
-A160A	12-05-16	+01:12:59.661	+15:29:28.695	3	900
-A0671	12-05-16	+08:28:31.843	+30:25:48.61	3	900
-A757	12-06-16	+09:13:07.904	+47:42:30.323	3	900
A2589	12-06-16	+23:23:57.426	+16:46:29.24	3	900
UGC03957	12-06-16	+07:40:58.366	+55:25:38.272	1	900
A2634	12-07-16	+23:38:29.225	+27:01:50.148	3	900

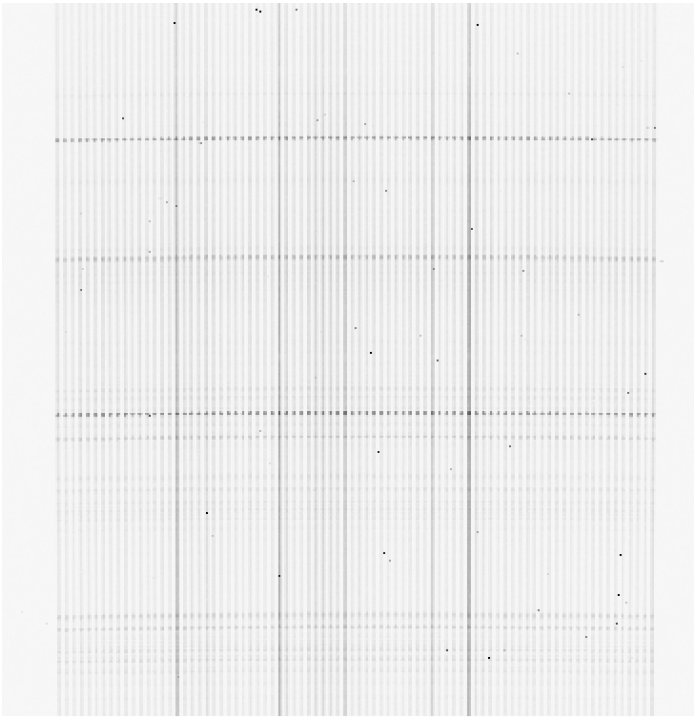

Figure 1. A raw image of the fibers from WIYN data from A160A. It has an exposure time of 900 seconds and is one of the original clusters specified in Table 1. This has not been corrected for the random noise that occurs.

Figure 2. A master image of the Bias of the CCD. A Bias/Zero image accounts for the inherent fluctuations of the CCD.

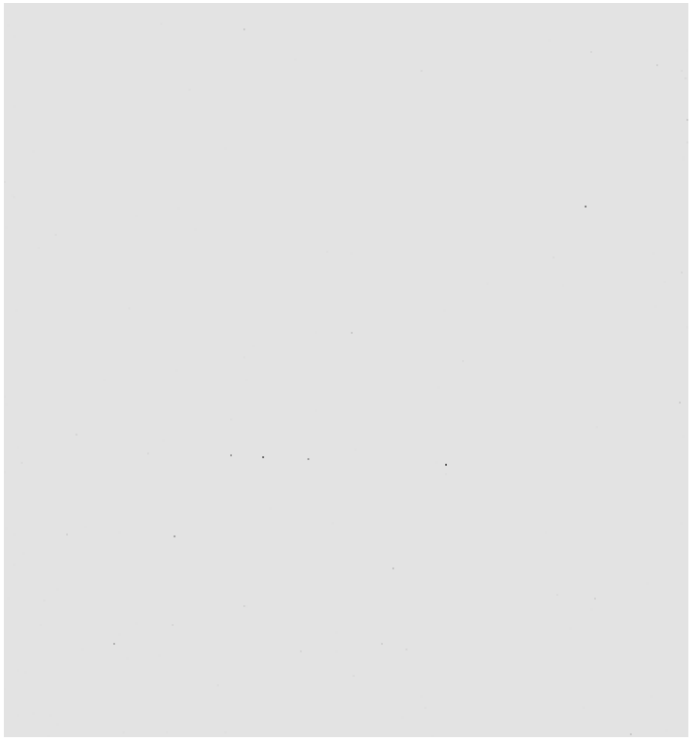

Figure 3. A master image of the 900 second Dark. This accounts for the random thermal fluctuations of the CCD.

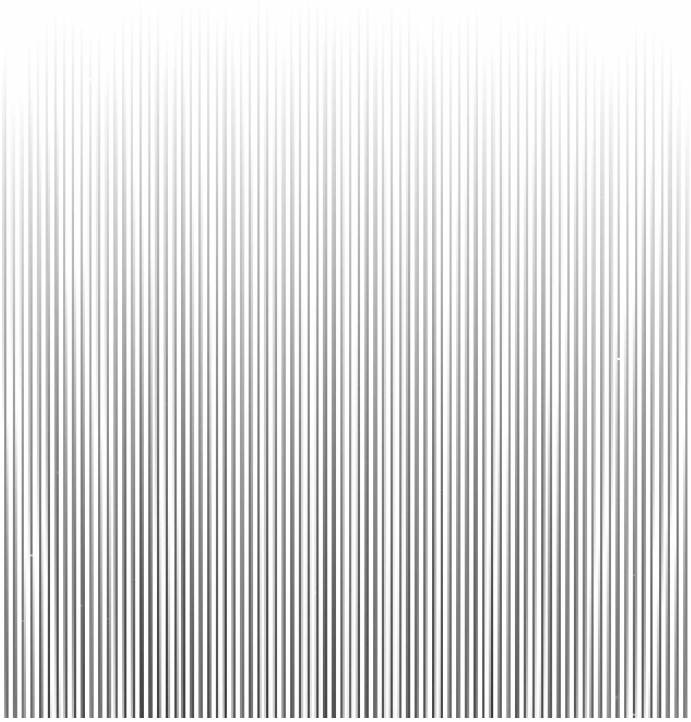

Figure 4. A master image of the Flats taken on 12/5/16. The Flat field master image can account for obstructions on the telescope, such as dust, or prints, and dark current in the CCD.

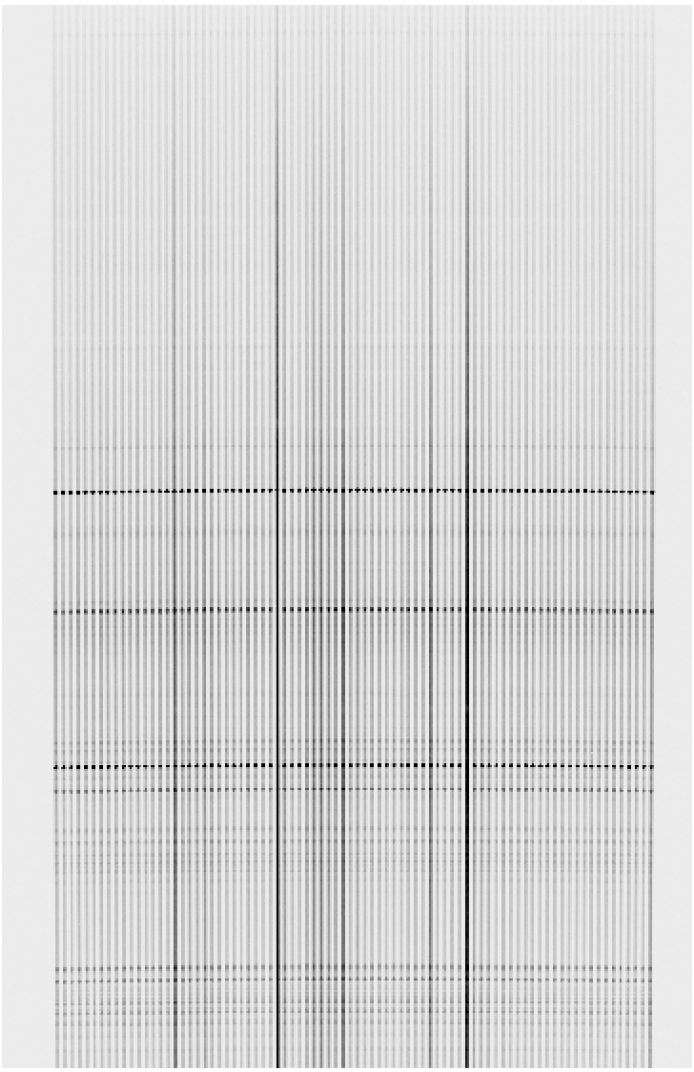

Figure 5. A calibrated image of A160A. It is a neater and cleaner image, compared to Figure 1.

Offset2 A0757. Steffanie, a colleague of the author's, did Home UGC03957, Home A2589, Home A2634 Offset1 A0671, Offset1 A2589, Offset1 A2634, Offset2 A2589, Offset2 A0671 and Offset2 A2634. Images that say "Home" are images taken when the telescope points to the coordinates provided in Table 1. "Offset1" and "Offset2" are new images that are dithered slightly, as to collect data from the whole BCG.

2.1.1 Preparing for Data Reduction: Putting into Lists

IRAF, Image Reduction and Analysis Facility, provided from NOAO, the National Optical Astronomy Observatory, was used to analyze every single fits file(the actual data). This is common procedure for data reduction taken via CCDs. Designated data files, FITS images, were organized into designated lists. The files had to match both the galaxy cluster name and the 3 positions of observation: Home, Offset1, or Offset2. For example, all the Home A602 images were in the same list, while Offset1 A0602 and Offset2 A0602 were in their own, different lists. There was total of 3 Home Lists, 2 Offset1 Lists, and 2 Offset2 Lists in Table 1; each list had a different galaxy cluster.

Lists were made for all the bias files, darks files, flats files, comps files, and images files. Doing this required the identification of the different types of images: those for calibration, and those that had data.

Bias images are zero second exposures that rid the raw data of minor impurities caused by the signal variations from the CCD. Dark images are images that have the same exposure time as that of the science data and subtract any noise caused by thermal related impurities on the CCD. Flat images are images that also have the same exposure time as your data images and rid the raw images from uneven distributions of light on the CCD. Comp images are images of stars with known qualities and characteristics in order to compare with the objects of interest for a specific night's atmosphere. The combination of accounting for these sources of noise in the raw images produce a clean, calibrated image free from unwanted and unnecessary noise.

2.1.2 Data Reduction

Next, all the bias images were combined to make a resulting average image, FullZero.fits image (Figure 2). The darks, with varying exposures, were combined with their respective integration times. There were various dark exposure times of 900 seconds, 10 seconds, 6 seconds and 5 seconds. Next, the zero correction is applied to the darks, creating FullDark.fits images, like Figure 3, with their respective exposure time. After applying the zero correction from FullZero.fits to the dark lists, new images were created, simulating images that had a 1 second exposure and 60 second exposure by dividing or multiplying the image. The function imarith was used to create those new FullDark.fits images, with exposures 1 and 60 seconds. The zero correction from the FullZero.fits and the FullDark.fits images was applied to the Flats, Comps, and Images Lists. The exposure times of the FullDark.fits images have to match the Flats, Comps, and Images exposure times. This is why imarith was used in the first place: to make corresponding exposure time images. Further, all the images in the FlatList were combined to make a FullFlat.fits (Figure 4 image, which is needed much later. All the images in the galaxy data lists(Home, Offset1, and Offset 2 lists) were combined to make an average image for each list. Cosmic rays were subtracted from the resulting average image using IRAF's "lacos".

This results in 2 new files, one that is a cleaned version of the average image without cosmic rays. (Figure 5) The other file is the Badpix.fits image. That image is from the bad pixels due to the remaining cosmic rays and the CCD.

After triple checking the names of input and output fits files were correctly typed and everything is correct, the 82 apertures of the CCD were able to be separated and accounted for separately. The FullFlat from earlier was used to separate the 82 apertures. After a series of windows and tasks to follow, the functions were changed slightly: coordli=linelists cuar.dat and select=match. The targetlist was first made for further use. The targetlist contained all Lacos files that was received from before.

In hydra in IRAF, and the parameters of dohydra were edited using "epar dohydra." The specific parameters that needed to be changed were changed on the following window. They include making the objects= @targetlist, apref= FullFlat.fits, flat= FullFlat.fits, and arcs1= the comp file. n1023.fits was the comp file used in this data reduction set. The gain and readnoise of the CCD were changed in "epar dohydra" as well.

The different wavelengths of the CuAr receiver were then identified. This was a long task but it showed promising results. This will be the file used from now on. The calibration of the wavelengths was stored in the database. It was named idn1023.fits.

Aperture 37 was missing. It might have been because another galaxy or star was in the spot of the aperture, which could have been filled with ICL. So, aperture 37 was added to the list of apertures that were outside of the central array, or those covered by other objects. This needed to be done for both Offsets 1 and Offsets 2, as well as the Home galaxies. For night 1, the author had 3 Home results, 2 Offset1 and 2 Offset2. This resulted in a total of 56 new files. For each galaxy, 7 were named for which aperture they corresponded with. One was named for the SkyFull, which was a combination of all the apertures for that galaxy. These 8 times 7 were the 56. The Lacos files from before were "subtracted" from the newly combined SkyFull image. This creates the Total image. This should be the data that has subtracted the atmosphere and light pollution. This total image will be important for later.

Table 2. Online Multi-wavelength datasets.

Name	Type	Telescopes	Website
NED	X-ray	ROSAT	https://ned.ipac.caltech.edu/forms/byname.html
NED	X-ray	Chandra	https://ned.ipac.caltech.edu/forms/byname.html
NED	X-ray	XMM	https://ned.ipac.caltech.edu/forms/byname.html
SDSS	Optical	SDSS	skyserver.sdss.org/dr13/en/tools/chart/navi.aspx
CADC	Optical	HST	www.cadc-ccda.hia-iha.nrc-cnrc.gc.ca
DSS	Optical	DSS	On DS9

Table 3. How to Untar/Unzip.

Untar/Unzip	Command
untar	tar -xvf[file name]
b unzip	bunzip2[file name]
g unzip	gunzip[file name]

2.2 Publicly Available Data Sets

As mentioned previously, there were a total of 23 clusters in this campaign. This project required higher resolution optical images, as well as X-ray data. As a result, data from various sources was gathered: the HST (the Hubble Space Telescope), the Chandra X-ray observatory, and XMM (X-ray Multi-Mirror Mission).

The 23 clusters were gathered from publicly available data through multiple databases. Table 2 lists the various databases and websites.

X-ray images of the galaxies were gathered from NED and the ROSAT and Chandra/XMM archives. The images were used to gather their positions and coordinates. Optical images of galaxies

Table 4. Different X-ray/Optical Pairs

X-ray	Optical
RASS	SDSS/SAO-DSS
RASS	HST
Chandra/XMM	SDSS/SAO-DSS
Chandra/XMM	HST

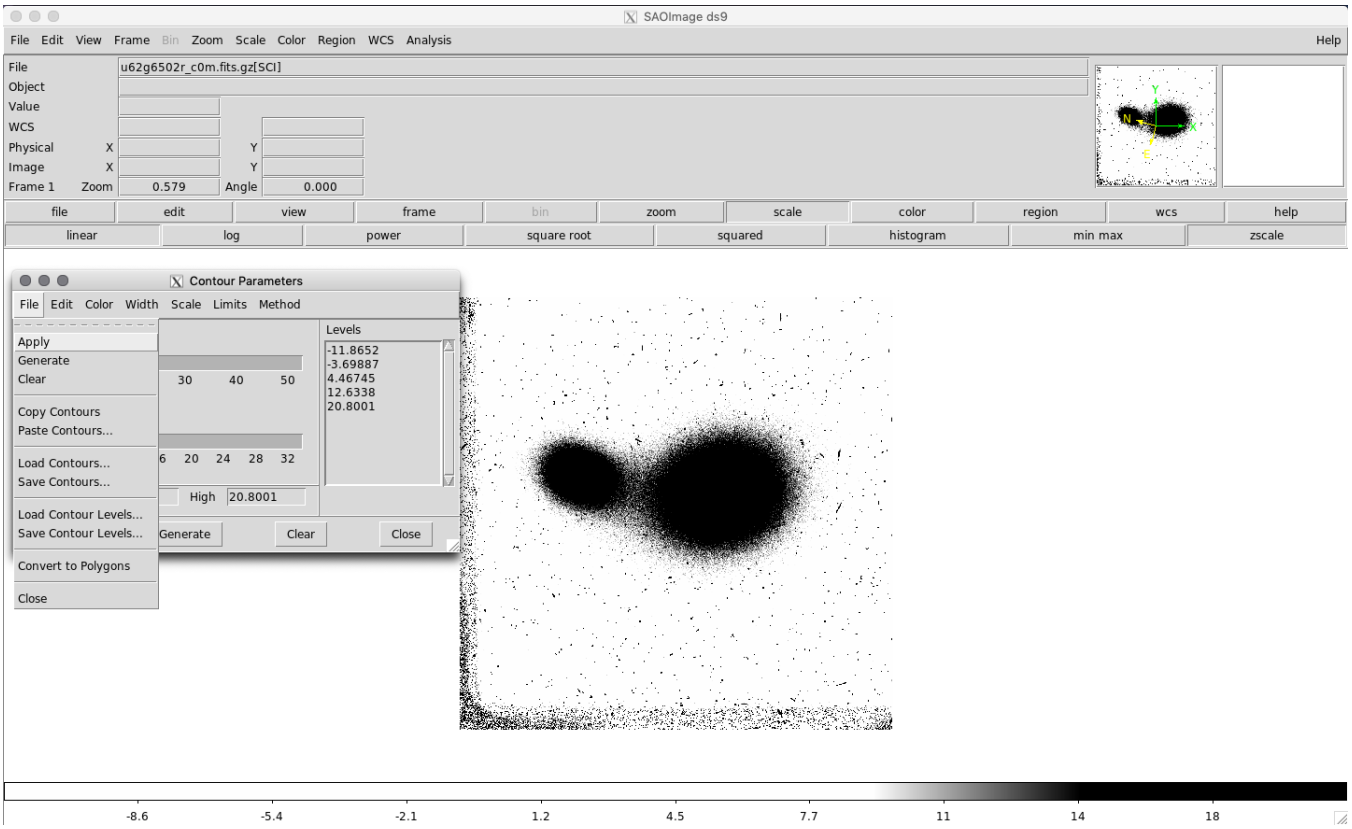

Figure 6. An Optical HST image of A2634, one of our initial objects on DS9 in z scale. This is an image that shows how to apply the contours from an X-ray image that can be created using the same drop down menu with an X-ray image that one desires to create contours for.

Table 5. Other Sparsepak Sample Galaxies

Cluster Names	RA	Dec
Abell 1668	+13:03:46.620	+19:16:17.47
Abell 1795	+13:48:52.515	+26:35:31.31
Abell 193	+01:25:07.598	+08:41:58.54
Abell 2199	+16:28:38.269	+39:33:06.47
Abell 2457	+22:35:40.808	+01:29:05.24
Abell 2622	+23:35:01.453	+27:22:20.10
Abell 2626	+23:36:30.504	+21:08:46.56
Abell 2665	+23:50:50.530	+06:08:58.52
Abell 376	+02:46:03.927	+36:54:18.52
Abell 407	+03:01:51.727	+35:50:23.23
Abell 75	+00:39:42.351	+21:14:05.18
Abell 85	+00:41:50.297	-09:18:10.33
IIZw108	+21:13:55.886	+02:33:54.91
MKW3s	+15:21:51.878	+07:42:32.48
Zw2844	+10:02:36.496	+32:42:24.79
Zw8338	+18:11:01.903	+49:54:42.33

from SDSS were also collected. The images were found from the corrected frame 'r' link upon searching for the cluster. The HST was the source for higher resolution and better quality optical images. These images were found at the Canadian Astronomy Data Centre. Preparing the data for overlaying X-ray contours required unzipping the ROSAT files or un-tarring the Chandra files. The commands to unzip and untar can be found in Table 3.

Table 6. Websites used for Python plotting and reading data

Name
https://matplotlib.org/users/pyplot_tutorial.html
https://www.youtube.com/watch?v=wAwQ-noyB98
http://www.astropy.org/astropy-tutorials/plot-catalog.html
http://docs.astropy.org/en/v0.2.1/coordinates/index.html
http://docs.astropy.org/en/stable/coordinates/
http://docs.astropy.org/en/stable/coordinates/matchsep.html

2.3 Creating X-ray contours and overlaying on Optical Images to find Centroids and Uncertainties

Here we discuss creating the X-ray contours and what was done with them.

DS9 is used to create contours that enable us to analyze the X-ray images. To get a good contour, different parameters like smoothness needed to be adjusted. Figure 6 and Figure 7 show a DS9 drop down menu of the Contour Parameters. This menu was used to create, edit, save, and load the X-ray contours onto optical images. The contours for each X-ray image were saved in order to overlay on multiple optical images. Saving contours is found in contour parameters setting. Load, found in the same spot as save, is used to load them on an optical image. The X-ray contours were then overlaid on top of the optical images in different combinations (see Table 4). Figure 8 and Figure 9 are optical images of A2634 in the zscale and min/max, respectively, with the X-ray contours overlaid on top of them.

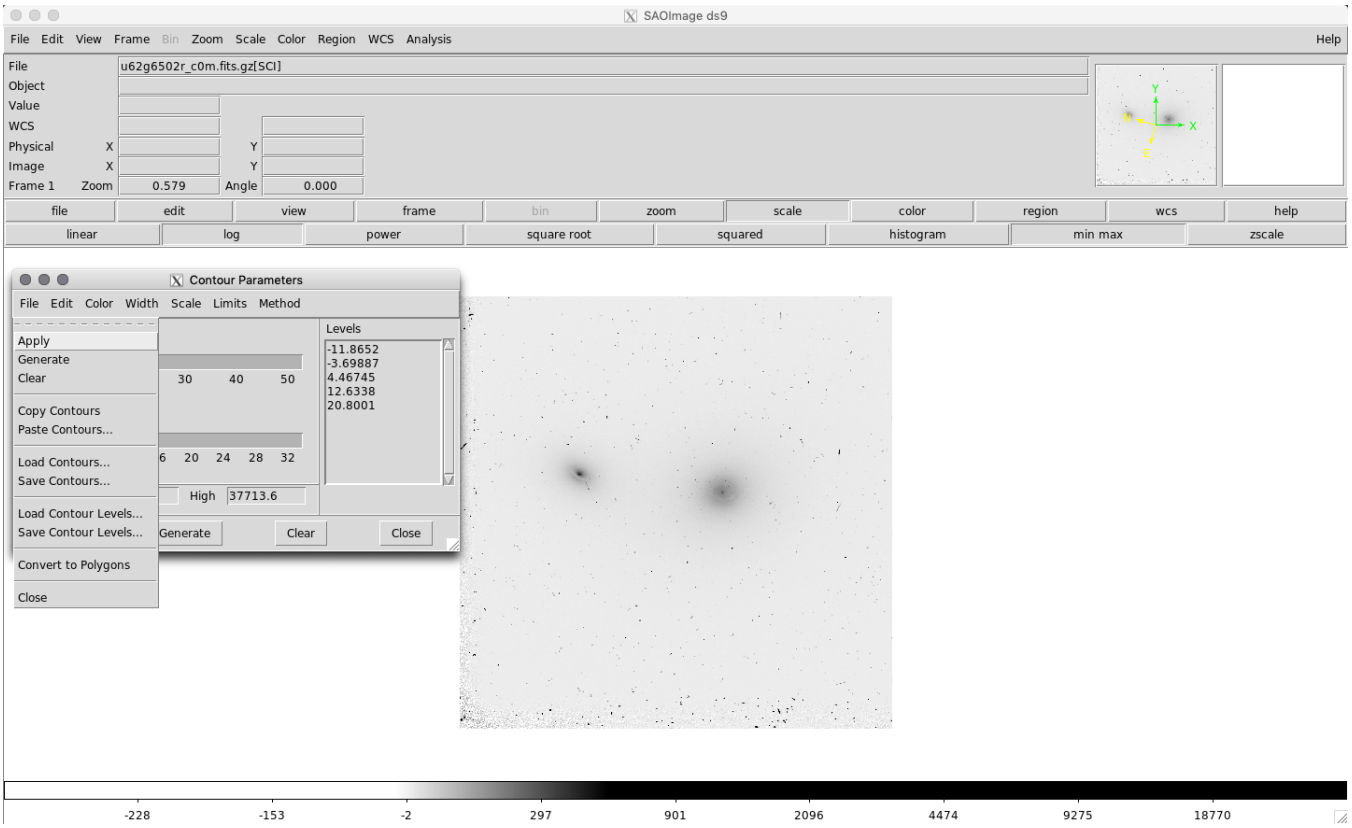

Figure 7. An Optical HST image of A2634, one of our initial objects on DS9 in min/max scale. This is an image that shows how to apply the contours from an X-ray image that can be created using the same drop down menu with an X-ray image that one desires to create contours for.

By having the contours loaded onto the image, the Right Ascension and Declination of the centroids of both the optical and X-ray light were identified. The centroids are used to figure out the separation between the two to help determine if there is any correlation with possible recent mergers it could have experienced.

This was done for all 23 galaxies in this campaign. The 7 BCGs this process was done on can be found in Table 1. The remainder 16 can be found inTable 5.

Most of the previously observed 16 clusters had Chandra images, but some lacked HST or SDSS data. Using Python, a full table using all 23 galaxies X-ray and optical centroids, uncertainties and separation was created. There is a Master Table that was created with all the data that was collected for all 23 galaxies, including Right Ascensions and Declinations. This can be found at the end of the document (Table 5).

Websites used for helpful information can be found in Table 6. The former being used for how to plot using Python. The latter used to help regarding reading coordinates in Python.

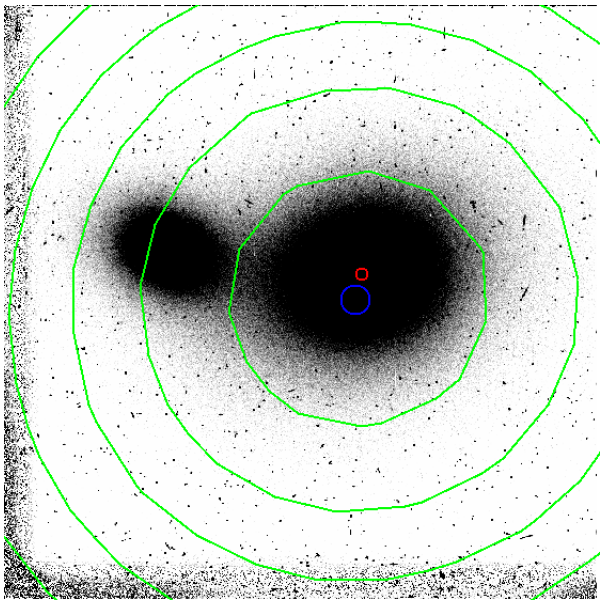

Figure 8. An Optical HST image of A2634, one of our initial objects on DS9 in z scale. This shows the HST image in the z scale with X-ray contours overlaid on top of the it. This was the goal for the 23 different galaxies, for all different combinations of Optical and X-ray sources (Table 4)

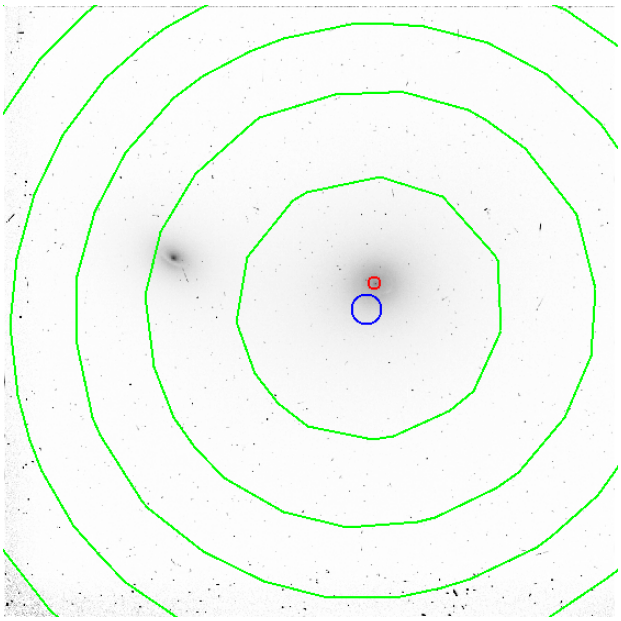

Figure 9. An Optical HST image of A2634, one of our initial objects on DS9 in min/max scale. This shows the HST image in the min/max scale with X-ray contours overlaid on top of the it. This was the goal for the 23 different galaxies, for all different combinations of Optical and X-ray sources (Table 4)

3 RESULTS

The uncertainty in separation of the cluster center and the galaxy center was also required. This requires finding uncertainty for the location of the centroid for both the X-ray and optical image. This was done by creating a circle on ds9 with the optical image and X-ray contours overlaid on them and finding the radius where the centroid of the X-ray contours or optical image might be located. What was first considered was having the same uncertainty for every source would be a good idea, and the preferred method. However, it may be the case that some of the contour parameters are different from when initially overlaid. So, even though the telescope may be the same, it might have different contour lines depending on the contour parameters, like smoothness and number of contours, and therefore different uncertainties. All the uncertainties were added to the 4 modified tables, one for every pair of sources. The Master Table (Table 5) was completed; it now contained all the correct centroids with their respective approximate uncertainties. Using Jupyter to interact with the Master Table, one can use it to make histograms of the data. In Jupyter, it was more advantageous to use Pandas to have the data as variables, as opposed to treating all the data as entire csv tables.

3.1 Finding Separation between centroids

After learning about Python plotting, and more about reading data, the Master Table from before could be interacted with using Jupyter. This was an achievement after some struggle because of the way Python read the table. Finding new ways to interact with the data was crucial due to its convenience. Creating tables, arrays, and columns/rows in Python using pandas was of most importances. Using pandas, one can single out one particular data point, say X-rayRA[0], the 1st entry of a column of X-ray RA centroids. The Astronomical Coordinate Systems on docs.astropy.org proved useful (Table 6).

Finding a way to convert the RA and Dec in sexigesimal to decimal degrees in order to find the difference/separation of the X-ray and optical centroids easier was attempted. The separation function was found; which was exactly what was needed for this project. It is used in all the different combinations of X-ray/optical pairs. Refer to the last row in Table 6 for the separation function. The separations were found using SkyCoord function on Astropy.

After converting to degrees, a new csv file without missing measurements was produced. For example, imagine there were no HST data for A75, the row of HST vs RASS or HST vs Chandra was not incorporated in this table. This made each table with each their own pair of Optical and X-ray data, without any gaps. This came from the master data table. These new csv files could now be read using Jupyter, a new project for each op/x pair.

All the images of the 50 pairs of sources that are represented on any of the 4 histograms were made. The images have a red circle indicating their Optical centroid and uncertainty, and the Blue circle indicates the X-ray centroid and uncertainty. The circles were created in DS9 and give a certain size based on the source they came from(HST had a smaller circle area compared to SDSS/SAO-DSS(Similarly, Chandra's circles were smaller than RASS's)).

The optical galaxy was first outlined with the circle in DS9. The circle was then shrunk so that it looked like it was at the core of the BCG. The same method was used for the X-ray circle. This was a little more complicated because the contours weren't always circular. Best judgement and the values of the X-ray image were employed and incorporated.

3.2 Visualizing the Separation using Histograms

Histograms for each different type of pairs: X-ray and optical were created. The offsets and histograms can be found in Figure 10. It is the number of galaxies that are separated by a certain amount of arcseconds/arcminutes. There are 4 different histograms for each pair running from different projects. The centroids are identified as the *peak* of the X-ray emission, and not an average of emission. The top left plot of Figure 10 is a histogram for objects with the Chandra/XMM and HST data, has 5 objects with both of these images. This was the best combination of sources because the resolution for Chandra and HST are better than RASS and SDSS respectively. The top right plot in Figure 10 has data that had both RASS and HST data. There was 6 objects that had this pair. The bottom left is a histogram that. depicts the separation of objects that had a SDSS or SAO-DSS source paired with Chandra or XMM. There was a total of 20 objects that shared this pair. The bottom right plot showed the objects that had a SDSS or SAO-DSS source paired with RASS. This was the least best pair of sources because of their bad resolutions. There was a total of 23 objects (all objects) with this pair.

Figure 11 is a histogram depicting the separation of a galaxy's best centroids. The order which we preferred were Chandra/XMM and HST, then Chandra/XMM and SDSS/SAO-DSS, followed by RASS and HST, and finally, RASS and SDSS/SAO-DSS. These centroids are identified as the *peak* of the X-ray emission, and not an average of emission. There were 23 galaxies that had both of images in those sources.

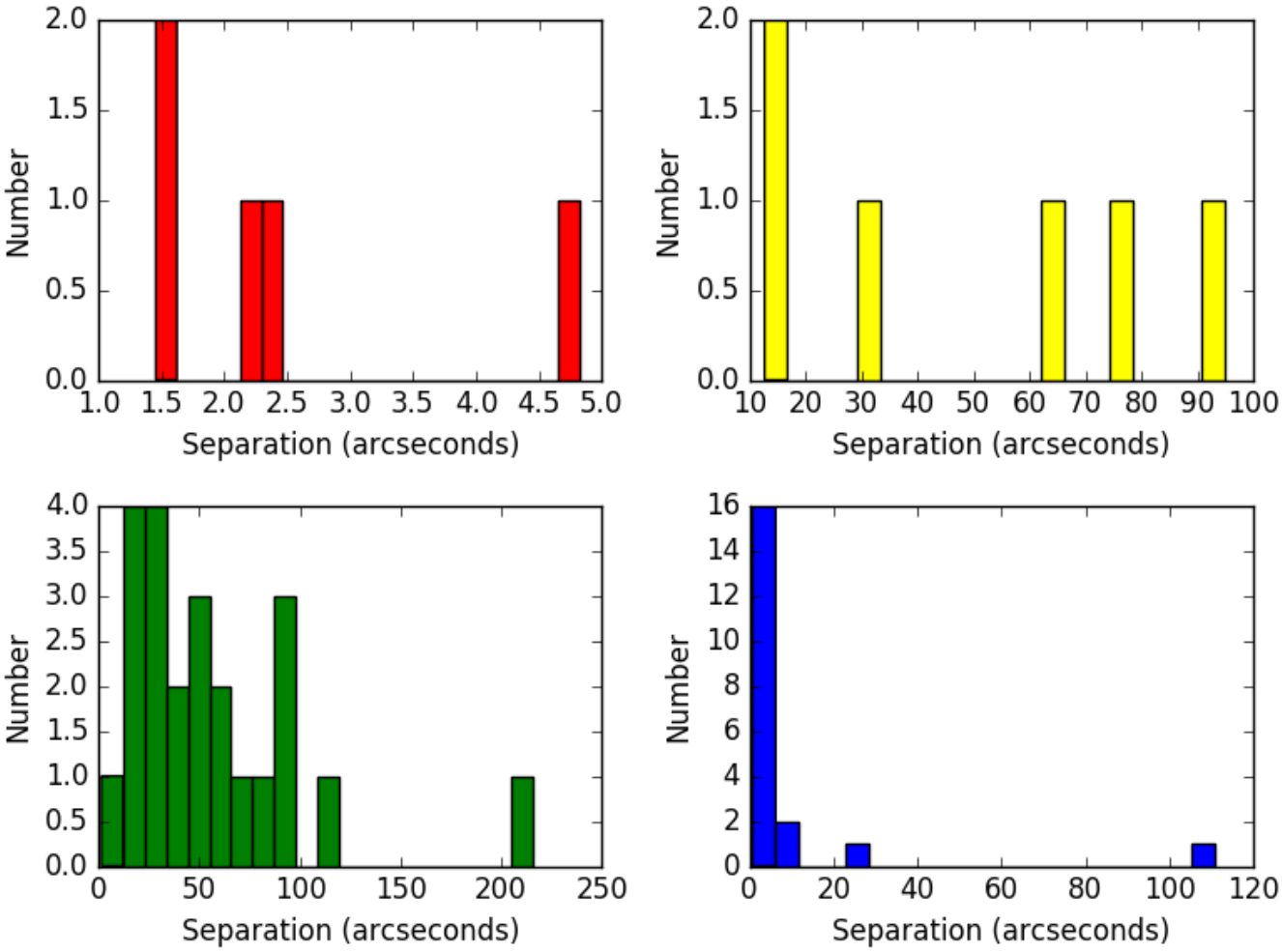

Figure 10. The initial 4 histograms created using Jupyter notebook and the centroids that were collected. The top left is the Chandra/XMM and HST pair, the top right is the RASS and HST pair, the bottom left is the Chandra/XMM and SDSS/SAO-DSS pair, and the bottom right is the RASS and SDSS?SAO-DSS pair.

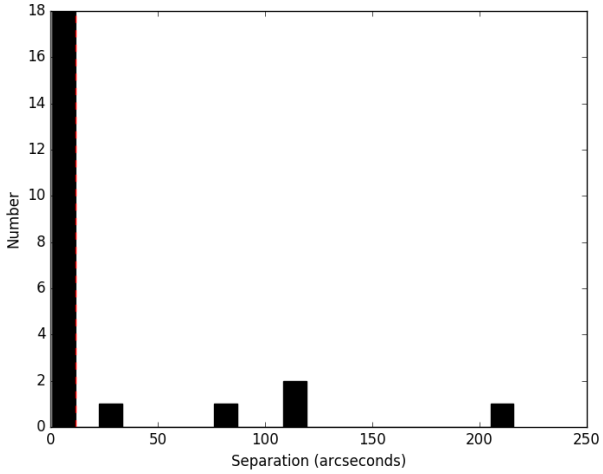

Figure 11. The final histogram I created in the Summer. This one has all the best sources for every cluster.

Table 7. Lakhchaura/Singh and Salinas common **Chandra** galaxies.

Cluster	Source	Right Ascension(J2000)	Dec(J2000)
Abell 193	LS	01:25:07.3	+08:41:36.0
	Salinas	01:25:07.497	+08:41:58.51
Abell 376	LS	02:45:48.0	+36:51:36.0
	Salinas	02:46:04.053	+36:54:20.28
Abell 2457	LS	22:35:40.3	+01:31:33.6
	Salinas	22:35:40.960	+01:29:07.12
Abell 2665	LS	23:50:50.6	+06:09:00.0
	Salinas	23:50:50.464	+06:09:00.98

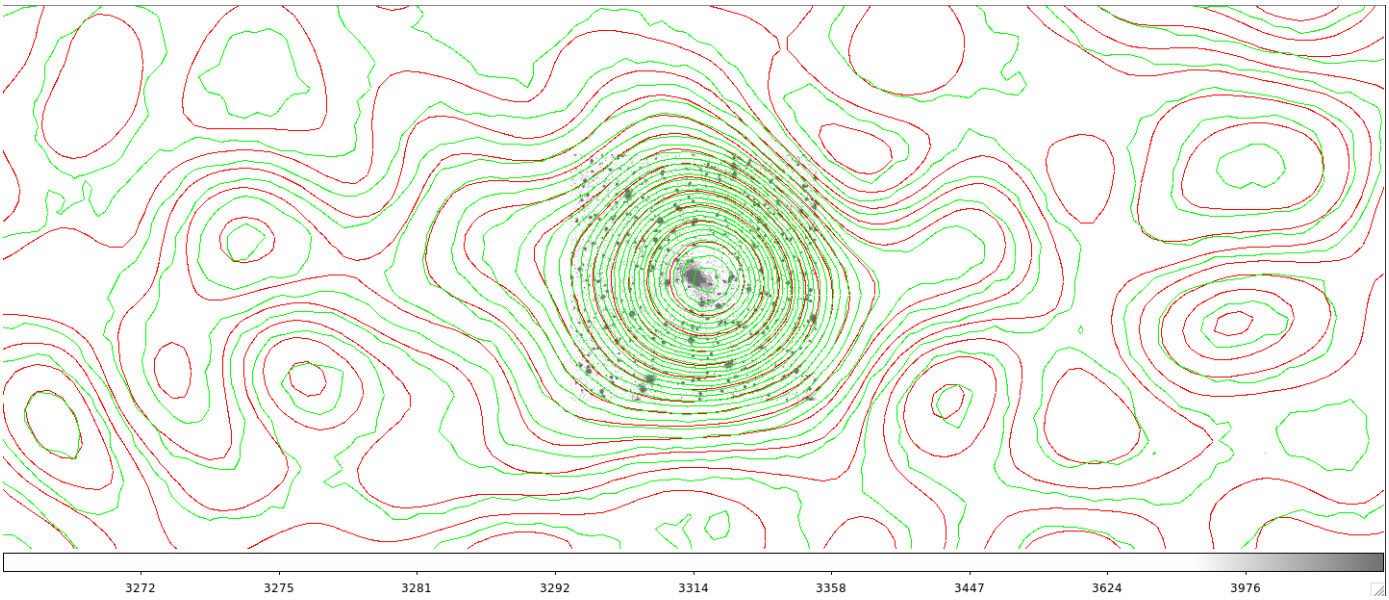

Figure 12. Further exploration caused me to discover that two clusters, the "outliers" were identified with a substructure included in their centroid, as compared to my "peak" centroid. This cluster is IIZw108.

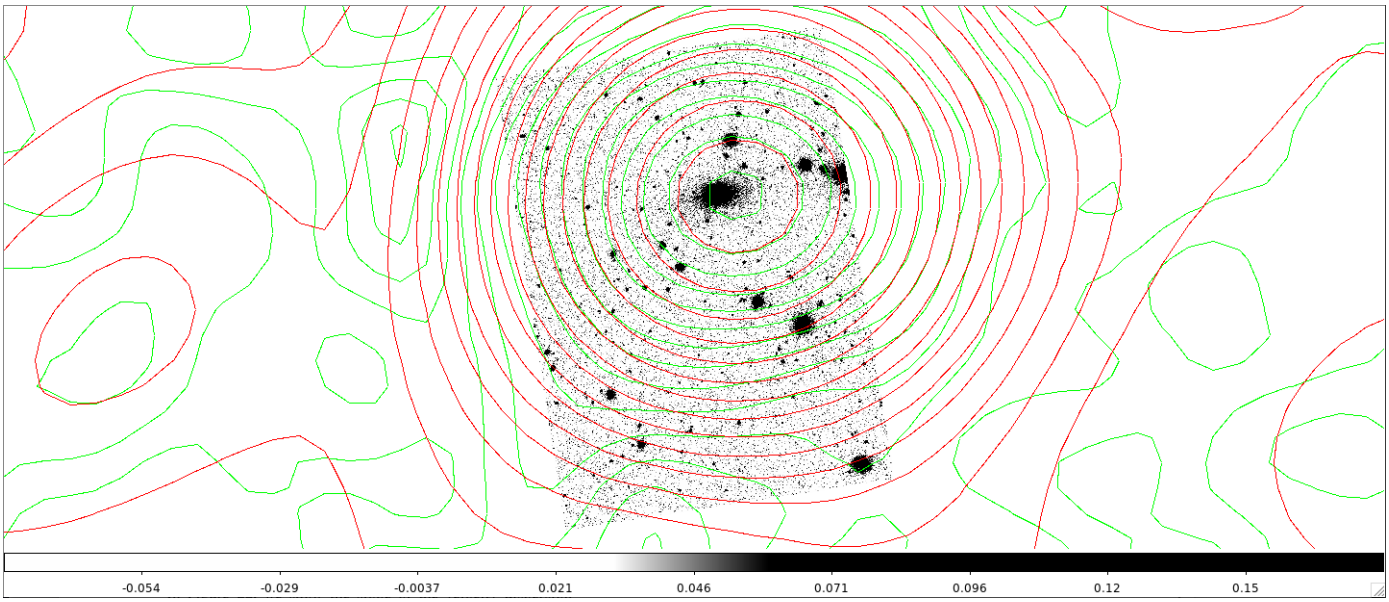

Figure 13. Further exploration caused me to discover that two clusters, the "outliers" were identified with a substructure included in their centroid, as compared to my "peak" centroid. This cluster is MKW3s.

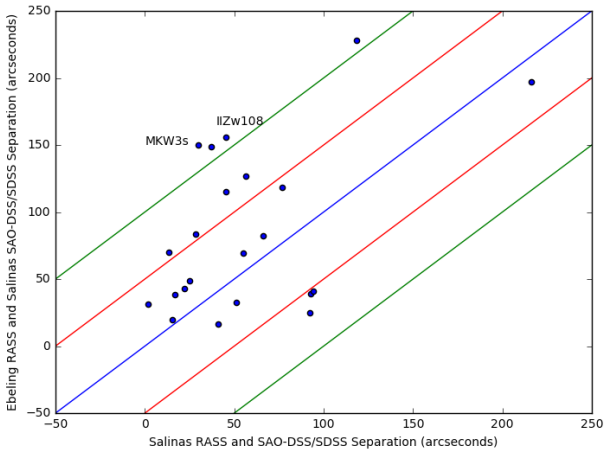

Figure 14. This graph compares the separation of Ebeling's RASS data and my optical compared to the separation of my RASS and optical. We can see several outliers which caused me to discover what was the cause for such a different separation. We found out that Ebeling included a substructure of 2 of the 4 outliers above the orange line. Figure 12 and Figure 13 include my contours of those clusters, and prove that there is a substructure included in Ebeling's data. To read more about this, check out the Ebeling Write up in Dirac.

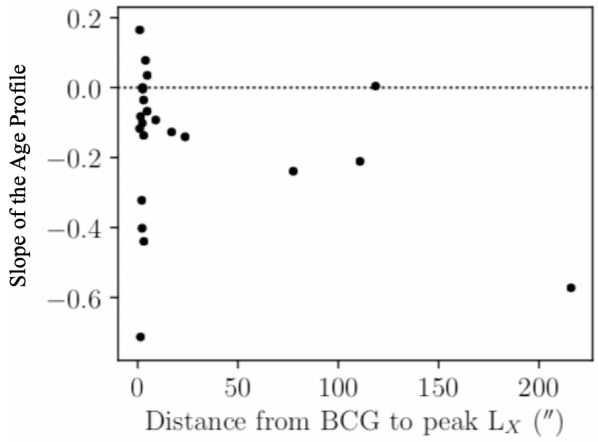

Figure 15. This is a plot Edwards et. al. 2019 (submitted) made showing the slope of the age profile versus the separation, distance from the optical centroid and the X-ray centroid, found in this paper. This plot may show a relationship between how old the BCG is and the separation.

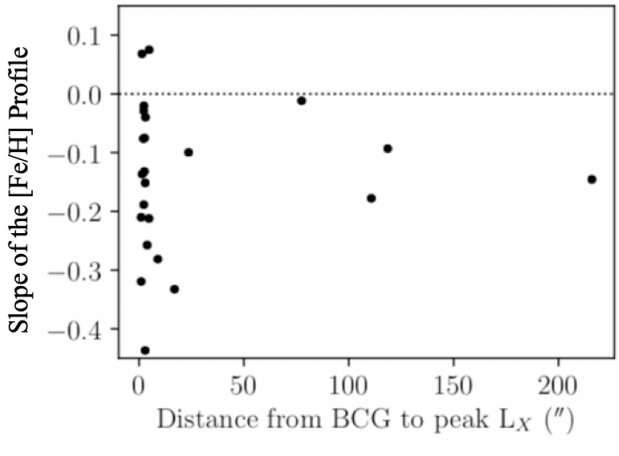

Figure 16. This is a plot Edwards et. al. 2019 (submitted) made showing the slope of the [Fe/H] profile versus the separation, distance from the optical centroid and the X-ray centroid, found in this paper. This plot may show a relationship between the Metallicity of the BCG and the separation.

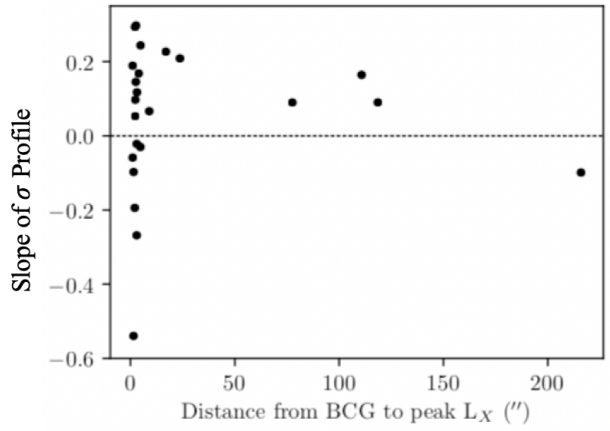

Figure 17. This is a plot Edwards et. al. 2019 (submitted) made showing the slope of the σ profile versus the separation, distance from the optical centroid and the X-ray centroid, found in this paper.

4 ANALYSIS

We will explore the offsets to see if there is a relationship between the age, velocity, or metallicity and the galaxy offset.

4.1 Comparison with Published Data

The separation of Ebeling's RASS to the Optical for HST and SAO-DSS or SDSS to the separation of my RASS and my Optical HST and SAO-DSS or SDSS data is discussed here. To verify our separations and X-ray centroids, we compared to previous work.

Figure 14 shows A2457, A75, IIZw108, and MKW3s had a large separation from the slope=1 line on the plot I created. To determine why, I recreated the contours of the RASS images, overlaid them on the same optical image, and adjusted their centroids, with the new contours. The issue persisted for three of the galaxies: A2457, IIZw108, and MKW3s, not A75. A75 found its way closer to the slope=1 line with the adjusted contours and adjusted centroid. Regardless, I saved the new images with the new contours and identified the centroid of the Ebeling RASS image with a yellow circle. I don't know where this error of X-ray centroid differed or began, but some possibilities could be the contours themselves (I made them from what seemed best, as maybe Ebeling had a certain process of how to create them).

Figure 14 is a plot showing the separation of my RASS data and my optical centroids with the separation of Ebeling's RASS data with my optical centroids. The orange line is a line that separates the accurate data with data that is otherwise. The 4 clusters that were above the orange line caused for further inspection. Figure 12 and Figure 13 show a zoomed out image of two of the outliers, IIZw108 and MKW3s, respectively, with their RASS X-ray contours overlaid on them. The yellow circles in both of these images identify Ebeling's centroids. The smaller blue and red circles are my optical and X-ray centroids, respectively. The yellow circles are toward the substructures in the X-ray contours.

The RASS centroids for Ebeling's data collection and my data collections didn't match. Figure 12 and Figure 13 were created to discover what is going on. For both figures, Ebeling's RASS centroid are translated a bit to the left of where the peak X-ray emission is. This may be because Ebeling included a separate X-ray substructure. This is due to the cluster not being as grouped together as the BCG is. Ebeling must have identified an average centroid of the cluster, while we defined the *peak* of X-ray emission as the cluster's centroid.

4.2 X-ray separation and gradients in Age, Redshift, and σ

The following figures are from Edwards et. al. 2019(in prep).

In Figure 15, we show the slope of the gradient of the age plotted against the distance from the BCG to the peak of the cluster X-ray luminosity. This plot may show any relationship with the separation and the lifetime of the BCG. This plot says that BCGs with large offsets between the *peak* of X-ray emission and the peak of visible light emission often have steep negative age gradients.

In Figure 16, we show the slope of the gradient in metallicity plotted against the distance from the BCG to the peak of the cluster X-ray luminosity. This plot may show any relationship with the separation and the metallicity of the BCG. This plot says that BCGs with large offsets between the peak of X-ray emission and the peak of visible light emission have small negative slopes, >-0.2.

In Figure 17, we show the slope of the velocity dispersion plotted against the distance from the BCG to the peak of the cluster X-ray luminosity. This plot may show any relationship with the separation and the velocity dispersion of the BCG. This plot says that BCGs with large offsets between the peak of X-ray emission and the peak of visible light emission have small positive slopes, nearing 0, one instance being below 0.

4.3 Relating "Disturbed" BCGs with traits from spectroscopy: ICL

The Intracluster Light (ICL) of the BCG is the light that surrounds the BCG and envelopes it within the cluster. This might mean that the ICL may not be directly associated with the BCG, but is within its gravitational influence. The ICL may be within the BCG outskirts.

Figure 18 is a figure that has 4 plots that relate the separation of the 23 BCGs and their host cluster and the BCG's intracluster light's (ICL) characteristics. On the top left is the velocity of the BCGs' ICL, on the top right is the velocity dispersion of the ICLs, the bottom left is the Age, and the bottom right is the metallicity. It may be difficult to make a claim about the velocity and velocity dispersion of the disturbed BCGs. Regarding Age: it is evident that BCGs with a large separation have a low age. This may coincide with how BCG mergers form. When a BCG collides with a smaller surrounding galaxy, the latter galaxy is absorbed within the BCG and triggers star formation within the ICL of the BCG. The metallicities of the largely separated BCGs all have a similarly high value, indicating that there are similar processes regarding star generation, formation, and evolution within the ICL of those BCGs.

4.4 Relating "Disturbed" BCGs with traits from spectroscopy: Core

Figure 19 is a figure that has 4 plots that relate the separation of the 23 BCGs and their host cluster and the BCG's core's characteristics. On the top left is the velocity of the BCGs' core, on the top right is the velocity dispersion of the cores, the bottom left is the Age, and the bottom right is the metallicity. There may be no statistically significant relationship between the core velocity and the separation of the BCG. This might not be of concern because when a BCG merges with a surrounding galaxy, we wouldn't expect that galaxy to disturb the kinematics of the core of the BCG. The same follows for the velocity dispersion of the BCG. Regarding age: it is hard to make a clear result from this plot. The typical age of the BCG core is high. Those with large separations - disturbed - may have a generally smaller age, but it's hard to confirm due to a small sample size. Disturbed BCGs have typical values of BCG core metallicities. This may indicate that galaxy mergers have no effect on the core's metallicity, which supports the typical BCG merger hypothesis.

5 CONCLUSION/FUTURE WORK

Learning about the evolution of Brightest Cluster Galaxies can assist us in finding the secrets of the universe. Through different light wavelengths, we can "see" and discover the dance between BCG and minor galaxies that are galaxy mergers. Gaining data via spectroscopy about BCGs allows us to know of the galaxy's composition and specific traits that are inherent to the BCG. Identifying the centroids of the different types of light from BCGs and their host cluster through creating X-ray contours and overlaying them on Optical images has proved to be useful for identifying the separations of these two values.

The separation of the two centroids tells us more about the

"state" (disturbed or undisturbed) of the BCG. By visualizing these separations through histograms, we could see the presence of these different states. After confirming our centroids and separations with previously published data, we have been better able to identify the means of how a cluster or galaxy is defined as.

By marrying the chemical compositions attained from the BCG spectra of the different areas of the BCG and the separations of the centroids of the visible and X-ray light, we can further understand the context of galaxy mergers a bit more.

Five of the 23 galaxies in this campaign were considered in a disturbed state. Being in a disturbed state meant having an Optical-X-ray centroid separation of 12.5 arcseconds or more. Of the 5, inference of how galaxy mergers with BCGs can be discovered. One of the interpretations of the data is that the disturbed BCG ICL is affected by a galaxy merger. The core of disturbed BCGs are minimally affected, if at all, by the galaxy merger. This corresponds to contemporary theory of galaxy formation and evolution. BCG core ages, velocities, velocity dispersions, and metallicities for disturbed galaxies have similar values compared to BCGs in undisturbed states. This implies that galaxy mergers with BCGs don't affect the core of the BCG. BCG ICL ages and metallicities for disturbed galaxies have different values compared to BCGs in undisturbed states. This implies that galaxy mergers with BCGs affect the ICL of the BCG. However, we also see no significant correlation between the separation and the BCG ICL velocities and velocity dispersions. This may be something to consider regarding the theory of galaxy formation.

Future work includes doing a similar project with the BCG's nearest companions. How does the BCG and its massive influence affect a nearby galaxy? How is the nearest companion of the BCG affected by the BCG's host cluster?

More future work includes involving the absolute magnitudes of the BCG and the nearest brightest object. In a similar fashion, how is the brightness and luminosity in neighboring galaxies affected by the presence of the BCG and its host cluster?

REFERENCES

Ebeling H., Edge A. C., Allen S. W., Crawford C. S., Fabian A. C., Huchra J. P., 2000, MNRAS, 318, 333

Ebeling H., Voges W., Bohringer H., Edge A. C., Huchra J. P., Briel U. G., 1996, MNRAS, 281, 799

Edwards L. O. V., Alpert H. S., Trierweiler I. L., Abraham T., Beizer V. G., 2016, MNRAS, 461, 230

Lakhchaura K., Singh K. P., 2014, AJ, 147, 156

Lauer T. R., Postman M., Strauss M. A., Graves G. J., Chisari N. E., 2014, APJ, 797, 82

Lavoie S. et al., 2016, MNRAS, 462, 4141

Table 8. Master Table

Name	X-ray Source	Op Source	X-ray RA	X-ray Dec	Op RA	Op Dec	X RA Uncert.	X Dec Uncert.	Op RA Uncert.
A0075	Ch/XMM	SAO-DSS	NaN	NaN	00:39:42.351	21:14:05.18	NaN	NaN	00:00:00.1
A0075	RASS	SAO-DSS	00:39:34.395	21:14:46.22	00:39:42.351	21:14:05.18	00:00:00.8	00:00:10	00:00:00.1
A0075	Ch/XMM	HST	NaN	NaN	NaN	NaN	NaN	NaN	NaN
A0075	RASS	HST	00:39:38.417	21:13:59.26	NaN	NaN	00:00:00.8	00:00:10	NaN
A0085	Chandra	SAO-DSS	00:41:50.426	-09:18:12.63	00:41:50.297	-09:18:10.33	00:00:00.06	00:00:00.6	00:00:00:3
A0085	RASS	SAO-DSS	00:41:48.645	-09:17:56.61	00:41:50.297	-09:18:10.33	00:00:00.5	00:00:07	00:00:00:3
A0085	Chandra	HST	00:41:50.422	-09:18:13.24	NaN	NaN	00:00:00.06	00:00:00.6	NaN
A0085	RASS	HST	00:41:48.645	-09:17:56.61	NaN	NaN	00:00:00.5	00:00:07	NaN
A0160A	Chandra	SDSS	01:13:00.375	15:29:08.14	01:12:59.586	15:29:28.89	00:00:00.2	00:00:03	00:00:00.3
A0160A	RASS	SDSS	01:13:03.704	15:30:39.30	01:12:59.586	15:29:28.89	00:00:01.5	00:00:18	00:00:00.3
A0160A	Chandra	HST	01:13:00.375	15:29:08.14	NaN	NaN	00:00:00.2	00:00:03	NaN
A0160A	RASS	HST	01:13:03.704	15:30:39.30	NaN	NaN	00:00:01.5	00:00:18	NaN
A0193	Chandra	SDSS	01:25:07.497	08:41:58.51	01:25:07.623	08:41:59.05	00:00:00.08	00:00:01	00:00:00.15
A0193	RASS	SDSS	01:25:07.569	08:41:45.86	01:25:07.623	08:41:59.05	00:00:00.3	00:00:04	00:00:00.15
A0193	Chandra	HST	01:25:07.497	08:41:58.51	01:25:07.598	08:41:58.54	00:00:00.08	00:00:01	00:00:00.05
A0193	RASS	HST	01:25:07.569	08:41:45.86	01:25:07.598	08:41:58.54	00:00:00.3	00:00:04	00:00:00.05
A0376	Chandra	SAO-DSS	02:46:04.053	36:54:20.28	02:46:03.927	36:54:18.52	00:00:00.04	00:00:00.5	00:00:00.1
A0376	RASS	SAO-DSS	02:46:01.854	36:53:18.41	02:46:04.045	36:54:19.17	00:00:00.6	00:00:06	00:00:00.1
A0376	Chandra	HST	02:46:04.053	36:54:20.28	02:46:03.927	36:54:18.52	00:00:00.04	00:00:00.5	00:00:00.02
A0376	RASS	HST	02:46:01.854	36:53:18.41	02:46:03.972	36:54:18.81	00:00:00.6	00:00:06	00:00:00.02
A0407	Chandra	SDSS	03:01:52.056	35:50:20.66	03:01:51.727	35:50:23.23	00:00:00.1	00:00:01	00:00:00.4
A0407	RASS	SDSS	03:01:50.880	35:49:33.16	03:01:51.727	35:50:23.23	00:00:00.5	00:00:04	00:00:00.4
A0407	Chandra	HST	03:01:52.056	35:50:20.66	NaN	NaN	00:00:00.1	00:00:01	NaN
A0407	RASS	HST	03:01:50.880	35:49:33.16	NaN	NaN	00:00:00.5	00:00:04	NaN
A0602	XMM	SDSS	07:53:21.175	29:22:58.86	07:53:26.669	29:21:34.53	00:00:00.35	00:00:04	00:00:00.25
A0602	RASS	SDSS	07:53:20.412	29:22:17.97	07:53:26.669	29:21:34.53	00:00:02	00:00:20	00:00:00.25
A0602	XMM	HST	07:53:21.175	29:22:58.86	NaN	NaN	00:00:00.35	00:00:04	NaN
A0602	RASS	HST	07:53:20.412	29:22:17.97	NaN	NaN	00:00:02	00:00:20	NaN
A0671	Chandra	SAO-DSS	NaN	NaN	08:28:31.664	30:25:51.55	NaN	NaN	00:00:00.3
A0671	RASS	SAO-DSS	08:28:37.570	30:25:58.96	08:28:31.664	30:25:51.55	00:00:01.5	00:00:18	00:00:00.3
A0671	Chandra	HST	NaN	NaN	08:28:31.596	30:25:52.21	NaN	NaN	00:00:00.15
A0671	RASS	HST	08:28:37.570	30:25:58.96	08:28:31.596	30:25:52.21	00:00:01.5	00:00:18	00:00:00.15
A0757	Chandra	SDSS	NaN	NaN	09:13:07.753	47:42:30.46	NaN	NaN	00:00:00.3
A0757	RASS	SDSS	09:13:28.905	47:41:58.33	09:13:07.753	47:42:30.46	00:00:02.5	00:00:15	00:00:00.3
A0757	Chandra	HST	NaN	NaN	NaN	NaN	NaN	NaN	NaN
A0757	RASS	HST	09:13:28.905	47:41:58.33	NaN	NaN	00:00:02.5	00:00:15	NaN
A1668	Chandra	SDSS	13:03:46.648	19:16:14.40	13:03:46.620	19:16:17.47	00:00:00.13	00:00:02	00:00:00.1
A1668	RASS	SDSS	13:03:46.712	19:16:18.39	13:03:46.620	19:16:17.47	00:00:00.8	00:00:04.5	00:00:00.1
A1668	Chandra	HST	13:03:46.648	19:16:14.40	NaN	NaN	00:00:00.13	00:00:02	NaN
A1668	RASS	HST	13:03:46.712	19:16:18.39	NaN	NaN	00:00:00.8	00:00:04.5	NaN
A1795	Chandra	SDSS	13:48:52.687	26:35:27.08	13:48:52.519	26:35:33.29	00:00:00.1	00:00:01	00:00:00.15
A1795	RASS	SDSS	13:48:53.460	26:35:41.67	13:48:52.519	26:35:33.29	00:00:00.6	00:00:06	00:00:00.15
A1795	Chandra	HST	13:48:52.687	26:35:27.08	13:48:52.515	26:35:31.31	00:00:00.1	00:00:01	00:00:00.05
A1795	RASS	HST	13:48:53.460	26:35:41.67	13:48:52.515	26:35:31.31	00:00:00.6	00:00:06	00:00:00.05
A2199	Chandra	SDSS	16:28:38.229	39:33:02.59	16:28:38.269	39:33:06.47	00:00:00.12	00:00:01	00:00:00.4
A2199	RASS	SDSS	16:28:36.237	39:32:32.75	16:28:38.269	39:33:06.47	00:00:00.5	00:00:05	00:00:00.4
A2199	Chandra	HST	16:28:38.229	39:33:02.59	NaN	NaN	00:00:00.12	00:00:01	NaN
A2199	RASS	HST	16:28:36.237	39:32:32.75	NaN	NaN	00:00:00.5	00:00:05	NaN
A2457	Chandra	SDSS	22:35:40.960	01:29:07.12	22:35:40.808	01:29:05.24	00:00:00.08	00:00:01	00:00:00.1
A2457	RASS	SDSS	22:35:41.796	01:28:31.20	22:35:40.808	01:29:05.24	00:00:00.7	00:00:07	00:00:00.1
A2457	Chandra	HST	22:35:40.960	01:29:07.12	NaN	NaN	00:00:00.08	00:00:01	NaN
A2457	RASS	HST	22:35:41.796	01:28:31.20	NaN	NaN	00:00:00.7	00:00:07	NaN
A2589	Chandra	SAO-DSS	23:23:57.462	16:46:37.94	23:23:57.404	16:46:38.56	00:00:00.25	00:00:03.1	00:00:00.16
A2589	RASS	SAO-DSS	23:23:56.653	16:45:42.93	23:23:57.404	16:46:38.56	00:00:01.5	00:00:22	00:00:00.16
A2589	Chandra	HST	23:23:57.462	16:46:37.94	NaN	NaN	00:00:00.25	00:00:03.1	NaN
A2589	RASS	HST	23:23:56.653	16:45:42.93	NaN	NaN	00:00:01.5	00:00:22	NaN
A2622	XMM	SDSS	23:35:01.264	27:22:20.58	23:35:01.453	27:22:20.10	00:00:00.03	00:00:00.3	00:00:00.15
A2622	RASS	SDSS	23:34:59.764	27:22:31.01	23:35:01.453	27:22:20.10	00:00:00.3	00:00:03	00:00:00.15
A2622	XMM	HST	23:35:01.264	27:22:20.58	NaN	NaN	00:00:00.03	00:00:00.3	NaN
A2622	RASS	HST	23:34:59.764	27:22:31.01	NaN	NaN	00:00:00.3	00:00:03	NaN

Table 8 – *continued* **Master Table**

Name	X-ray Source	Op Source	X-ray RA	X-ray Dec	Op RA	Op Dec	X RA Uncert.	X Dec Uncert.	Op RA Uncert.
A2626	Chandra	SDSS	23:36:30.347	21:08:46.52	23:36:30.342	21:08:45.79	00:00:00.04	00:00:00.4	00:00:00.1
A2626	RASS	SDSS	23:36:28.864	21:09:05.40	23:36:30.342	21:08:45.79	00:00:00.3	00:00:03	00:00:00.1
A2626	Chandra	HST	23:36:30.347	21:08:46.52	23:36:30.504	21:08:46.56	00:00:00.04	00:00:00.4	00:00:00.02
A2626	RASS	HST	23:36:28.864	21:09:05.40	23:36:30.504	21:08:46.56	00:00:00.3	00:00:03	00:00:00.02
A2634	Chandra	SAO-DSS	23:38:29.469	27:01:53.48	23:38:29.364	27:01:52.37	00:00:00.122	00:00:01.6	00:00:00.3
A2634	RASS	SAO-DSS	23:38:24.577	27:00:43.51	23:38:29.364	27:01:52.37	00:00:02	00:00:25	00:00:00.3
A2634	Chandra	HST	23:38:29.469	27:01:53.48	23:38:29.361	27:01:53.68	00:00:00.122	00:00:01.6	00:00:00.1
A2634	RASS	HST	23:38:24.577	27:00:43.51	23:38:29.361	27:01:53.68	00:00:02	00:00:25	00:00:00.1
A2665	Chandra	SDSS	23:50:50.464	06:09:00.98	23:50:50.530	06:08:58.52	00:00:00.03	00:00:00.3	00:00:00.1
A2665	RASS	SDSS	23:50:49.831	06:09:17.86	23:50:50.530	06:08:58.52	00:00:00.15	00:00:02	00:00:00.1
A2665	Chandra	HST	23:50:50.464	06:09:00.98	NaN	NaN	00:00:00.03	00:00:00.3	NaN
A2665	RASS	HST	23:50:49.831	06:09:17.86	NaN	NaN	00:00:00.15	00:00:02	NaN
IIZw108	Chandra	SDSS	21:13:56.019	02:33:55.97	21:13:55.886	02:33:54.91	0:00:00.15	00:00:1.5	00:00:00.15
IIZw108	RASS	SDSS	21:13:52.923	02:33:45.847	21:13:55.886	02:33:54.91	00:00:00.5	00:00:07	00:00:00.15
IIZw108	Chandra	HST	21:13:56.019	02:33:55.97	NaN	NaN	0:00:00.15	00:00:1.5	NaN
IIZw108	RASS	HST	21:13:52.923	02:33:45.847	NaN	NaN	00:00:00.5	00:00:07	NaN
MKW3s	Chandra	SDSS	15:21:51.603	07:42:24.49	15:21:51.878	07:42:32.48	00:00:00.1	00:00:01.5	00:00:00.1
MKW3s	RASS	SDSS	15:21:49.842	07:42:30.76	15:21:51.852	07:42:31.77	00:00:00.3	00:00:04	00:00:00.1
MKW3s	Chandra	HST	15:21:51.603	07:42:24.49	NaN	NaN	00:00:00.1	00:00:01.5	NaN
MKW3s	RASS	HST	15:21:49.842	07:42:30.76	NaN	NaN	00:00:00.3	00:00:04	NaN
UGC03957	Chandra	SAO-DSS	07:40:58.276	55:25:38.31	07:40:58.160	55:25:35.35	00:00:00.02	00:00:00.15	00:00:00.3
UGC03957	RASS	SAO-DSS	07:40:56.374	55:25:42.81	07:40:58.160	55:25:35.35	00:00:00.7	00:00:07	00:00:00.3
UGC03957	Chandra	HST	07:40:58.276	55:25:38.31	NaN	NaN	00:00:00.02	00:00:00.15	NaN
UGC03957	RASS	HST	07:40:56.374	55:25:42.81	NaN	NaN	00:00:00.7	00:00:07	NaN
Zw2844	XMM	SDSS	10:02:36.355	32:42:23.75	10:02:36.496	32:42:24.79	00:00:00.05	00:00:00.5	00:00:00.1
Zw2844	RASS	SDSS	10:02:40.786	32:42:13.86	10:02:36.496	32:42:24.79	00:00:01.5	00:00:15	00:00:00.1
Zw2844	XMM	HST	10:02:36.355	32:42:23.75	NaN	NaN	00:00:00.05	00:00:00.5	NaN
Zw2844	RASS	HST	10:02:40.786	32:42:13.86	NaN	NaN	00:00:01.5	00:00:15	NaN
Zw8338	Chandra	SAO-DSS	18:11:01.857	49:54:41.38	18:11:01.903	49:54:42.33	00:00:00.02	00:00:00.2	00:00:00.1
Zw8338	RASS	SAO-DSS	18:10:57.513	49:54:57.78	18:11:01.903	49:54:42.33	00:00:00.4	00:00:04	00:00:00.1
Zw8338	Chandra	HST	18:11:01.857	49:54:41.38	NaN	NaN	00:00:00.02	00:00:00.2	NaN
Zw8338	RASS	HST	18:10:57.513	49:54:57.78	NaN	NaN	00:00:00.4	00:00:04	NaN

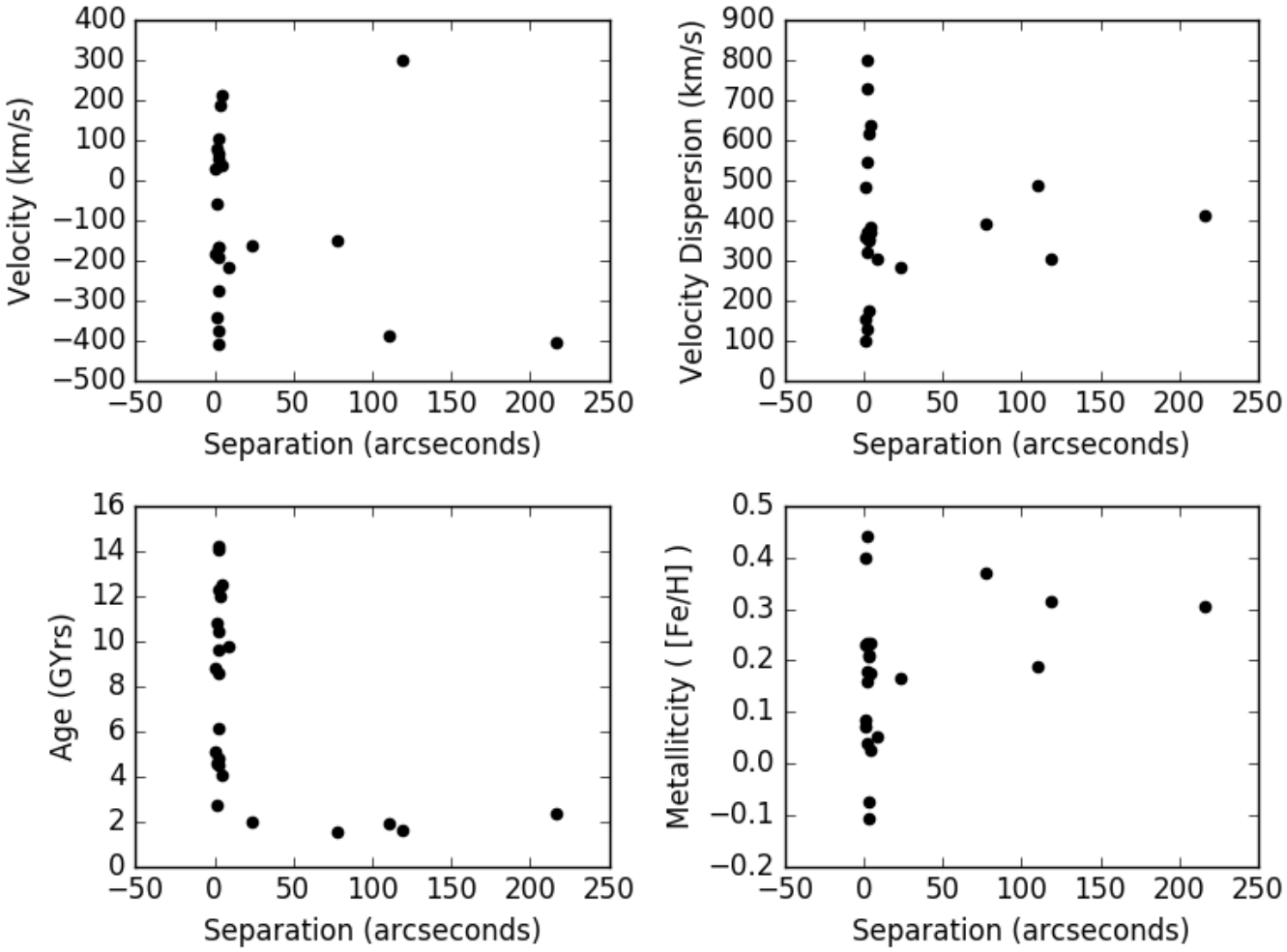

Figure 18. This is a plot of the BCG's ICL Velocity (Top Left), Velocity Dispersion (Top Right), Age (Bottom Left), and Metallicity (Bottom Right) received from Dr. Edwards versus the separation, distance from the optical centroid and the X-ray centroid, found in this paper. These plots show that there may be a relationship between the ICL's characteristics of the BCG and their separations.

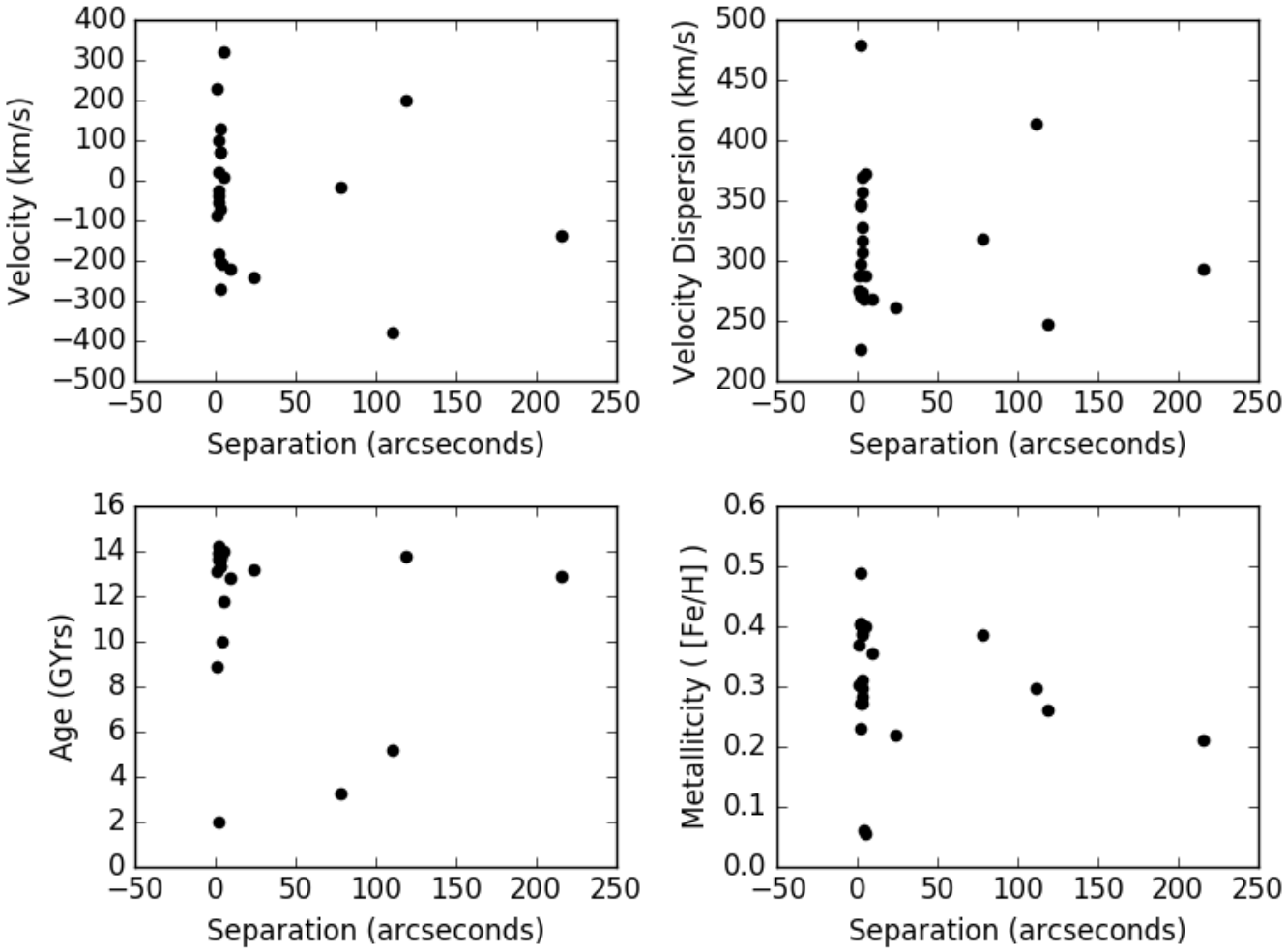

Figure 19. This is a plot of the BCG's Core Velocity (Top Left), Velocity Dispersion (Top Right), Age (Bottom Left), and Metallicity (Bottom Right) received from Dr. Edwards versus the separation, distance from the optical centroid and the X-ray centroid, found in this paper. These plots show that there may be a relationship between the core's characteristics of the BCG and their separations.